First Images of a Glutamate Receptor Ion Channel: Oligomeric State and Molecular Dimensions of GluRB Homomers†

Markus Safferling,‡,§ Willem Tichelaar,‡ Günther Kümmerle,‡ Annukka Jouppila,|| Arja Kuusinen,|| Kari Keinänen,|| and Dean R. Madden*,‡

Ion Channel Structure Research Group, Max Planck Institute for Medical Research, Jahnstrasse 29, 69120 Heidelberg, Germany, and Viikki Biocenter, Department of Biosciences (Division of Biochemistry) and Institute of Biotechnology, Post Office Box 56, FIN-00014 University of Helsinki, Helsinki, Finland

Received June 4, 2001; Revised Manuscript Received September 5, 2001

ABSTRACT: We have expressed, purified, and characterized glutamate receptor ion channels (GluR) assembled as homomers of the subunit GluRB. For the first time, single-milligram quantities of biochemically homogeneous GluR have been obtained. The protein exhibits the expected pharmacological profile and a high specific activity for ligand binding. Density-gradient centrifugation reveals a uniform oligomeric assembly and a molecular mass suggesting that the channel is a tetramer. On the basis of electron microscopic images, the receptor appears to form an elongated structure that is visualized in several orientations. The molecular dimensions of the molecule are approximately 11 × 14 × 17 nm, and solvent-accessible features can be seen; these may contribute to formation of the ion-conducting pathway of the channel. The channel dimensions are consistent with an overall 2-fold symmetric assembly, suggesting that the tetrameric receptor may be a dimer of dimers.

The ionotropic glutamate receptors (GluR)[1] are ligand-gated cation channels of the central nervous system, where they play an important role in both physiological and pathological processes (reviewed in ref *1*). Pharmacologically distinct subfamilies of GluR have been identified. GluR with high affinity for AMPA (α-amino-5-methyl-3-hydroxy-4-isoxazole propionate) are responsible for most fast excitatory synaptic signaling in the brain. Recent evidence also implicates the AMPA receptors in the activity-dependent modulation of synaptic strength (reviewed in ref *2*).

AMPA receptors are formed by homo- or heterooligomers of the subunits GluRA−D (also known as GluR1−4) (*3*−*5*). The GluRB subunit is particularly important in determining the ion permeability characteristics of the channels: receptors containing GluRB have a very low calcium permeability compared to those not containing it (*6*). Interactions of the cytoplasmic C-terminus of GluRB with proteins of the postsynaptic density appear to play a key role in the targeting and localization of GluR ion channels (*7*) but not in the assembly of functional channels (*8*).

The direct structural information currently available for the AMPA receptors is a series of crystallographic structures of the core of the ligand-binding domain of GluRB, representing ∼25% of the molecular mass of the complete subunit (*9*). Little structural information is available on the interdomain and intersubunit interactions that are presumably important for GluR activation and desensitization. The oligomeric state of the glutamate receptors has also not been definitively established (reviewed in ref *1*), although recent evidence suggests a dimer-of-dimers model (*8*).

While functional insect-cell expression of GluRD and GluRB/D ion channels and purification of GluRD AMPA receptor homomers have been previously reported, the purified protein exhibited levels of aggregation unacceptable for structural studies (*10*, *11*; unpublished data). Here, we report the milligram-scale expression and purification of affinity-tagged GluRB AMPA receptors, optimized for ligand-binding activity, yield, and structural homogeneity. The resulting material permits assessment of the channel's stoichiometry and characterization of its gross structural features and molecular dimensions.

EXPERIMENTAL PROCEDURES

Plasmid and Baculovirus Generation. Affinity-tagged cDNA containing the flop isoform of the rat GluRB subunit (SWISS-PROT accession number P19491, ref *4*) was assembled by PCR techniques in a pFastBac1 derivative harboring a baculoviral signal peptide (ecdysteroid UDP-glucosyltransferase), fused to a FLAG epitope (*12*) and a cloning linker (RPHAMG). The vector also contained a C-terminal hexahistidine tag (*13*), preceded by a four-residue linker (MNSR). The C- and N-terminal tags are used for immobilized metal-affinity chromatography (IMAC) and immunoaffinity purifications, respectively, of the recombinant GluRB homomers. Correctness of all PCR-derived sequences was verified by DNA sequencing. The construct

† Financial support was provided in part by EU Grant BIO4-CT96-0589 of the Fourth Framework Program in Biotechnology (D.R.M. and K.K.), the Max Planck Society (D.R.M.), and the Academy of Finland (K.K.).

* Corresponding author: Telephone +49-6221-486150; fax +49-6221-486437; e-mail madden@mpimf-heidelberg.mpg.de.

‡ Max Planck Institute for Medical Research.

§ Present address: Skirball Institute, New York University Medical Center, 540 First Ave., New York, NY 10016.

|| University of Helsinki.

[1] Abbreviations: GluR, ionotropic glutamate receptor; AMPA, α-amino-5-methyl-3-hydroxy-4-isoxazole propionate; MOI, multiplicity of infection; PMSF, phenylmethanesulfonyl fluoride; TX-100, Triton X-100; IMAC, immobilized metal-affinity chromatography.

10.1021/bi011143g CCC: $20.00
Published on Web 10/26/2001

omits the native C-terminal Ile residue of $GluRB_{flop}$ and thus corresponds to residues 1−861 of the mature sequence. Recombinant baculovirus v506-2 was generated using the Bac-to-Bac protocol (Gibco), and amplified in *Spodoptera frugiperda* Sf21 cells.

Cell Culture and Protein Expression. For initial characterization, Sf21 cells were infected and harvested as described for GluRD (*11*). Large-scale cell culture was performed in shaker flasks. Protein expression was performed in Sf21 or *Trichoplusia ni* High Five insect cells infected with multiplicity of infection (MOI) ≥ 4 in Ex-cell 400 medium (JRH Biosciences), and viral expansion was performed in Sf9 cells in TNM-FH medium supplemented as described (*14*). Cell viability was assayed 86 h after infection by staining with trypan blue (Gibco). If the viability was <95% or cells had lost their round and uniformly clear appearance, they were harvested. Otherwise they were left shaking for another 4 h.

Cell Harvest and Lysis. All further steps were performed at 4 °C. Cells were harvested by use of a Contifuge 20 S, equipped with rotor type 8684 and a Pericor CD 240 peristaltic pump (Heraeus), at 2100*g* (4000 rpm) and a flow rate = 280 mL min^{-1}. Alternatively, cells were centrifuged at 1500*g* for 10 min. The cell pellet was washed with 300 mL of TBS (150 mM NaCl and 50 mM Tris, pH 7.4) containing 0.1 mM phenylmethanesulfonyl fluoride (PMSF; Sigma) and then resuspended in 100 mL of lysis buffer (20 mM HEPES pH 7.4, and 5 mM EDTA), supplemented with 0.1 mM PMSF and Complete protease inhibitor tablets (one tablet dissolved in 500 mL of buffer; Roche Molecular Biochemicals). The suspension was divided into 16 aliquots, each of which was homogenized with a Polytron 1200 C (Kinematica) for 3 × 10 s at 5000 rpm. Tubes were incubated on ice between pulses. Each tube was then filled with an additional 30 mL of lysis buffer and the membranes were pelleted at 31000*g* for 30 min. The pellet was resuspended and centrifuged twice more, the first time in lysis buffer and then in 20 mM HEPES, pH 7.4, 200 mM NaCl, and 0.5 mM EDTA, each supplemented with PMSF and Complete protease inhibitors as above. This treatment lysed ≥99% of all cells, as determined by visual inspection.

Receptor Solubilization. Pellets were pooled and suspended in 250 mL of solubilization buffer [20 mM HEPES, pH 7.4, 200 mM NaCl, and 10% (v/v) glycerol], supplemented with PMSF and Complete protease inhibitors as above. The protein concentration was determined by bicinchoninic acid assay (Pierce). The solubilizate was diluted to ≤4 mg/mL protein with solubilization buffer, typically to a final volume of 2 L for a large-scale prep. Triton X-100 (TX-100; Roche Molecular Biochemicals; purified for membrane protein research) was added to 1.5% (v/v). The suspension was mixed for 90 min with a Reax-20 overhead mixer (Heidolph) at 4 rpm, and clarified by centrifugation, either at 75600*g* for 30 min or at 185000*g* for 15 min.

Immobilized Metal-Affinity Chromatography. Chelating Sepharose fast flow (Pharmacia, 10 mL) was charged essentially as described (*11*) with Zn^{2+}, Ni^{2+}, or Co^{2+}. Before loading, the clarified solubilizate was adjusted to 1 M NaCl and 5 mM imidazole. The suspension was gently mixed for 12 h at 4 rpm. Subsequently, the resin was recovered by filtration through a 500 mL glass frit (medium porosity; Schott). The Sepharose was washed with 5 column volumes (CV) of 20 mM HEPES, pH 7.4, 10% glycerol, and 0.1% TX-100 (buffer A) containing 1 M NaCl and 10 mM imidazole, followed by wash steps with buffer A containing first 200 mM NaCl and 10 mM imidazole (3 CV), then 100 mM NaCl and 10 mM imidazole (3 CV), and finally 100 mM NaCl and 50 mM imidazole (5 CV). GluRB was eluted in buffer A containing 100 mM NaCl and steps of 100 (5 CV), 200 (5 CV), and 500 (10 CV) mM imidazole. These eluates were analyzed by SDS−PAGE, and GluRB-containing fractions were pooled to give a typical final volume of 200 mL for a large-scale prep. Protein bands in silver-stained gels were quantitated with 1D Image Analysis software (Kodak Digital Science).

Immunoaffinity Chromatography. M1 α-FLAG affinity gel (IBI Kodak/Sigma, 3 mL) was equilibrated in M1 buffer (TBS supplemented with 3 mM $CaCl_2$ and 0.1% TX-100). Pooled GluRB-containing fractions from the IMAC column were adjusted to 3 mM $CaCl_2$ and applied to the gel at 0.5−1 mL min^{-1}. After the column was washed with 20 CV of M1 buffer, GluRB was eluted in 20 CV of TBS containing 500 mM NaCl, 10% glycerol, 0.1% TX-100, and 10 mM EDTA. The protein concentration was determined by Amido Black assay (Bio-Rad). Pooled M1 eluates (typically 60 mL) were concentrated by use of Centriplus-100 concentrators (Millipore) or Nanosep-100 concentrators (Pall-Filtron).

Ligand-Binding Assay. Binding assays were performed as described (*11*), with 25−50 μg of protein per reaction. Protein activity was quantified as described (*11*), except that 15 nM [^{3}H]AMPA (Dupont-NEN) was used. In competition binding assays, the concentration of radioligand was 5 nM, IC_{50} values were determined by nonlinear curve fitting to a model for one-site binding (GraFit, Erithacus Software; Prism, GraphPad Software), and apparent affinities (K_i) were determined by use of the Cheng−Prusoff equation (*15*).

Glycerol Density-Gradient Centrifugation. Analysis was performed in a linear, 20−80% (v/v) glycerol density gradient in TBS and 0.1% TX-100 (total volume 9.5 mL). GluRB (50 μg in 0.5 mL) as well as the reference proteins thyroglobulin, apoferritin, and alcohol dehydrogenase (500 μg in 0.5 mL) were centrifuged in an Optima LE-80K centrifuge using a Ti67 rotor (Beckman) for 16 h at 180000*g* (37000 rpm) at 4 °C. Fractions of 0.5 mL were collected. GluRB was quantitated by [^{3}H]AMPA binding assay. Protein standards were quantitated by the method of Bradford (*16*).

Electron Microscopy. Purified GluRB (3 μL) was applied to hydrophilic carbon films at a concentration of 20 μg mL^{-1}. The grid was washed with two droplets of 25 mM Tris, 20 mM NaCl, and 2 mM EDTA, pH 7.4, stained with 2% uranyl acetate and 0.1% glucose, and air-dried. The preparation was performed at 4 °C. Images were recorded at a nominal magnification of 50000× with a Zeiss CEM 902 operating at 80 kV, with an electron dose of ∼10 $e^-/Å^2$ and discarding electrons scattered inelastically with an energy loss greater than about 15 eV. The objective lens defocus was chosen such that the first reversal of the phase contrast transfer function was at ∼0.05 $Å^{-1}$. The negatives were digitized with a Zeiss SCAI scanner at a resolution of 21 μm.

The single particle image analysis was carried out essentially according to Schatz et al. (*17*) and Serysheva et al. (*18*) in the context of the IMAGIC-5 software system (*19*). More than 10 000 single-molecular images were selected. They were aligned with the "alignment by classification" approach (*20*), by which bias toward any specific reference

Table 1: Ligand-Binding Pharmacology of Recombinant GluRB Expressed in Sf21 Cells

ligand	K_d (nM)	IC_{50}[a] (μM)	K_i[b] (μM)
AMPA	16.8 ± 2.3		
L-Glutamate		0.50 ± 0.01	0.39 ± 0.01
kainate		4.7 ± 0.5	3.6 ± 0.4
CNQX[c]		0.28 ± 0.04	0.21 ± 0.03

[a] IC_{50} is the concentration required to displace 50% of radioligand binding. [b] K_I is the apparent affinity (*15*). [c] CNQX is 6-cyano-7-nitroquinoxaline-2,3-dione.

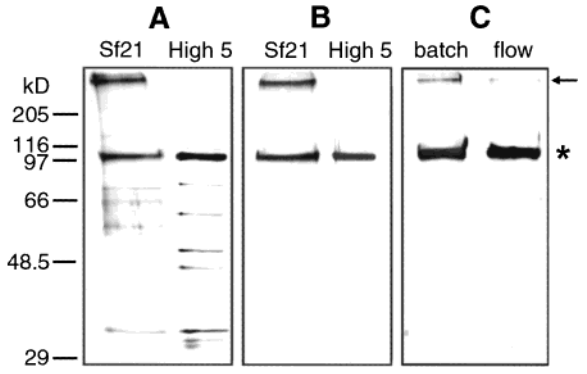

FIGURE 1: Comparison of GluRB expression conditions. (A, B) GluRB expressed in different insect cell lines, after purification by metal-chelate and immunoaffinity chromatography. (A) Silver stained SDS−polyacrylamide electrophoretic gel; (B) M1α-FLAG Western blot of GluRB samples isolated from Sf21 and High Five cells. (C) M1α-FLAG Western blot of GluRB from High Five cells harvested by conventional batch centrifugation (left lane) or continuous-flow centrifugation (right lane). In each comparison, equal fractions of the purified protein were loaded. The asterisk indicates the GluRB monomer band; the arrow marks the position of GluRB that did not enter the gel.

image is avoided. Class averages resulting from this procedure were used as the starting set of reference images for iterative cycles of multireference alignment (MRA), multivariate statistical analysis (MSA), and classification. One-fifth of the molecular images were discarded in the classification, and the average number of members per class was 25. The MRA−MSA−classification procedure was iterated until stable classes were obtained.

RESULTS

Protein Expression. Sf21 cells infected with the GluRB-encoding baculovirus v506-2 produced a ~100-kDa band by SDS−PAGE that immunoreacted with a FLAG-specific antibody. This band was not observed in uninfected cells nor in cells infected with wild-type AcNPV baculovirus (data not shown). Cell membranes prepared from v506-2-infected Sf21 cells showed specific and high-affinity binding of [^{3}H]-AMPA and a ligand-binding pharmacology typical of GluRB (Table 1) (*21*).

We next compared expression in Sf21 cells with that in High Five insect cells, which are suitable for the expression of a variety of membrane proteins (*22*) and for large-scale production (*14*). Equal volumes of Sf21 and High Five cells were infected with v506-2 at MOI = 5 and harvested 90 h later. Protein was purified by metal-chelate and α-FLAG immunoaffinity chromatography and analyzed by SDS−PAGE and Western blotting (Figure 1A,B). The yield from High Five cells was 85 μg/L, significantly higher than the 25 μg/L obtained with Sf21 cells. Moreover, protein obtained with Sf21 cells showed an obvious high molecular mass band in both the silver-stained gel and the Western blot, reflecting partial aggregation (Figure 1A,B, arrow). Protein obtained from High Five cells exhibited much less aggregation, although some was occasionally detectable in highly developed Western blots (e.g., Figure 1C). Overall, the data suggest that High Five cells produce larger amounts of GluRB and provide an environment in which the ion channel is less prone to aggregation than Sf21 cells.

GluRB expression levels were then monitored as a function of the conditions of infection in High Five cells. The time course of radioligand binding was monitored during the course of infection and reached a maximum 86 h postinfection. The falloff in AMPA binding was rather sharp on either side of the optimal time point t_{max}. Twenty-four hours before and after t_{max}, AMPA binding was 30% and 50% less than the maximum, respectively. The ligand-binding activity of cells infected at different MOI showed maximal expression for MOI ≥ 3. In practice, the MOI was chosen between 4 and 5.

We also compared batch and continuous-flow centrifugation methods for cell harvest, since experience with seven-transmembrane helical proteins had indicated that continuous-flow centrifugation was advantageous in avoiding premature cell lysis (G. Schertler, personal communication). The yield of GluRB from cells harvested by continuous-flow centrifugation was 134 μg/L, somewhat higher than the value obtained from the same batch of infected cells harvested with conventional batch centrifugation (104 μg/L). In addition, the continuous-flow approach further reduced the slight GluRB aggregation detected with the batch method (Figure 1C).

Purification of the Receptor. Having optimized conditions for the overexpression and harvest of GluRB, we next attempted to improve the purification scheme. The construct contains a C-terminal hexahistidine tag and an N-terminal FLAG epitope, so initial purifications used a Ni^{2+} column followed by α-FLAG immunoaffinity chromatography. However, the immunoaffinity eluates exhibited several contaminants (Figure 1A). The purity of the IMAC eluates was very poor when Ni^{2+} was used as the cation (Figure 2A, right-hand panel), and some of these contaminants evidently coeluted with GluRB during immunoaffinity chromatography (Figure 2B, right-hand panel, lanes e1 and e2). To improve the initial IMAC purification, Zn^{2+} and Co^{2+} were investigated as alternative cations. The use of Zn^{2+} instead of Ni^{2+} dramatically reduced contamination in the IMAC eluates and permitted the isolation of essentially pure material following immunoaffinity purification (Figure 2A,B, left-hand panels). It also resulted in elution of GluRB at somewhat lower imidazole concentrations than observed with Ni^{2+}. The yield at this step was typically ~80%. The use of Co^{2+} had an intermediate effect.

The optimized protocol has been reproducibly used in preparations at the 16 L scale. SDS−PAGE analysis of each step of a large-scale purification is shown in Figure 2C. In the final sample, GluRB is detected as a single band with an apparent molecular mass of 104 kDa, without indication of aggregation. This corresponds to the predicted amino acid sequence (99.1 kDa) together with ~4.9 kDa of glycosylation (at up to four potential N-linked glycosylation sites). Yields

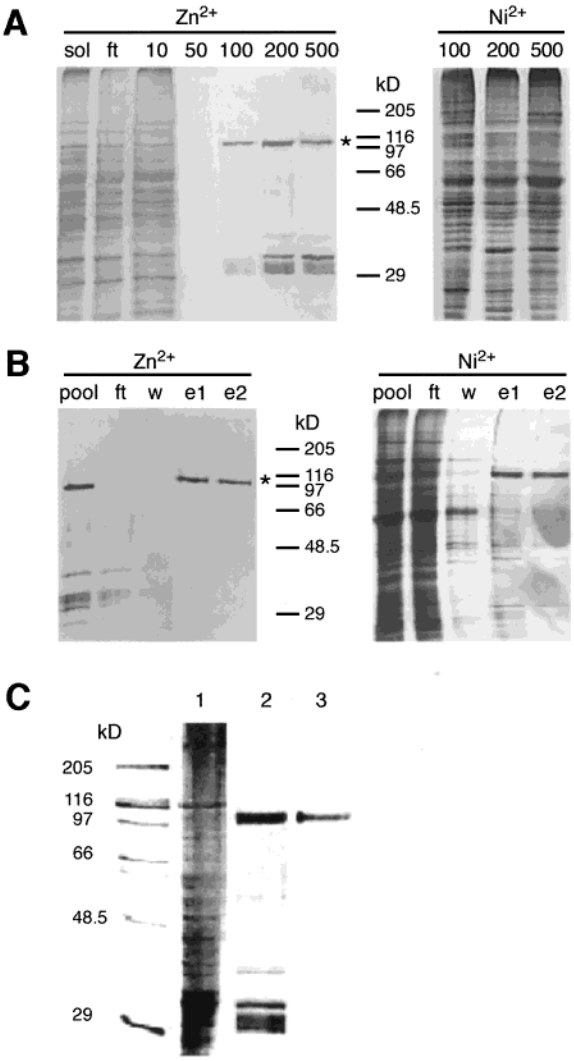

FIGURE 2: Purification of GluRB. (A, B) Role of metal-affinity cations. Silver-stained SDS−polyacrylamide electrophoretic gels are shown for the IMAC (A) and immunoaffinity (B) purification steps, with either Zn^{2+} or Ni^{2+} as cations. (A) IMAC. For Zn^{2+}, solubilized membrane proteins (sol) are shown, together with column flowthrough (ft) and wash/elution steps at various imidazole concentrations (millimolar). For Ni^{2+} only eluate fractions are shown. The asterisk marks the expected GluRB molecular mass. (B) Immunoaffinity purifications. For each cation, the pooled IMAC eluates (pool), the column flowthrough (ft), column wash (w), and two 10 mM EDTA eluates (e1 and e2) are shown. (C) Overview of final GluRB purification on a silver-stained SDS−polyacrylamide electrophoretic gel. Lane 1, Triton X-100 solubilized insect-cell membranes; lane 2, pooled IMAC eluates (Zn^{2+}); lane 3, pooled immunoaffinity eluates. Lanes in panel C are from separate gels.

at this scale were consistently in the range of 80−130 μg of highly purified GluRB/L of cells.

Biochemical Characterization. The purified, solubilized receptor had a K_D of 18.2 ± 0.9 nM for [^{3}H]AMPA and a B_{max} of 2140 pmol/mg of GluRB, as assayed by filter binding. Since filter binding is a nonequilibrium technique, the reported capacity does not necessarily reflect the specific activity of the protein. To establish approximately what fraction of GluRB is active, we performed filter-binding experiments with soluble GluRD ligand-binding domains known to exhibit ~100% specific activity by equilibrium dialysis measurements (*23*). Using the soluble construct, we

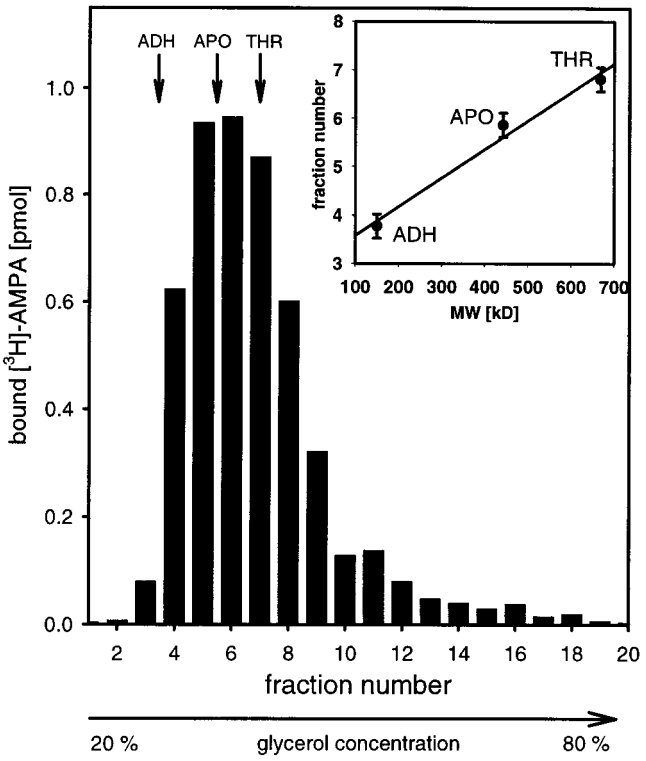

FIGURE 3: Density gradient centrifugation of Triton X-100-solubilized GluRB. The protein was quantitated by radioligand binding (bar graph). Standard proteins used for the calibration of the gradient (arrows above graph and inset) were thyroglobulin (THR, 669 kDa), apoferritin (APO, 443 kDa), and alcohol dehydrogenase (ADH, 150 kDa).

obtained a filter-binding signal that was consistently ≤20% of the theoretical maximum. Assuming that filter-binding studies detect a similar fraction of GluRB binding sites, the true number of AMPA binding sites would be close to the theoretical maximum of ~10 000 pmol/mg, for one agonist molecule per monomer.

Purified GluRB is assembled in a uniform oligomeric state as determined by density gradient centrifugation in glycerol (Figure 3) and sucrose (not shown). Its distribution in the gradient can be described as a single peak with a possible, small higher molecular-mass shoulder (fraction 11, Figure 3). The molecular mass of the GluRB complex was calibrated relative to soluble proteins (Figure 3, inset), yielding a value of 495 kDa. The GluRB peak is only slightly broader than those of the standard proteins, with a half-width of ~5 fractions, vs ~4 fractions for apoferritin.

Electron Microscopy. Purified GluRB homomers were negatively stained with uranyl acetate and visualized by electron microscopy (Figure 4A). Individual particles of uniform size are observed in several different orientations. More than 10 000 single molecular images were selected, aligned, classified, and averaged to improve the signal-to-noise ratio. Five out of a total of 155 class averages are shown in Figure 4C, together with corresponding single molecular images (Figure 4B). Since the molecule is elongated, the projections vary in appearance from approximately round to extended. The projected dimensions correspond to a molecule with a long dimension of 17 nm and a perpendicular cross section of 11 × 14 nm. The particle also is indented or hollow, i.e., it contains internal solvent-

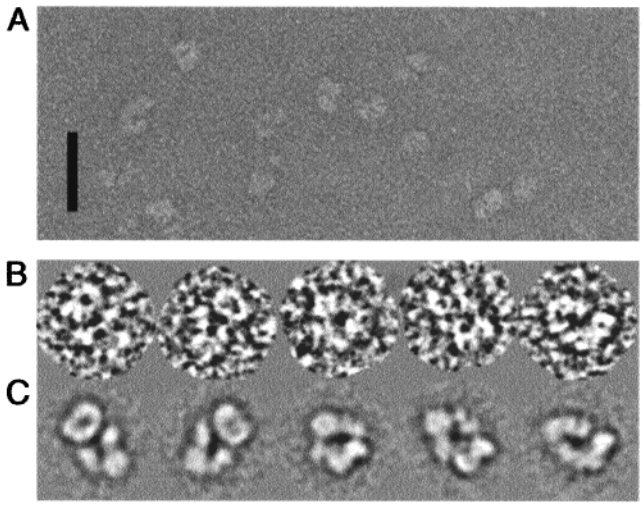

FIGURE 4: Electron microscopic images of negatively stained GluRB. (A) Representative field from an electron micrograph of negatively stained single particles. Scale bar, 50 nm. (B, C) Classification and averaging of single particles of GluRB. (B) Single particle images that were assigned to five different classes (of a total of 155), together with corresponding class averages (C). In panels B and C, the edge of one frame corresponds to 27 nm.

accessible volumes seen as stain-filled structures within the molecular outlines of the class averages. Equivalent features are seen in the unaveraged images, albeit with the expected lower signal-to-noise ratio.

DISCUSSION

A major barrier to structural and functional studies of membrane proteins that are not naturally abundant is the difficulty of expressing the required milligram quantities with the required homogeneity and functionality (reviewed in ref *22*). Here we report a system for the expression and purification of a homomeric GluRB ion channel that addresses several of these issues. This has permitted us to characterize the channel's hydrodynamic properties and to determine its overall structure and molecular dimensions by electron microscopy.

Several factors were essential in obtaining receptor preparations of the high biochemical quality required. The purity of the GluRB preparation was decisively influenced by the use of Zn^{2+} rather than Ni^{2+} or Co^{2+} cations during metal-chelate chromatography. This contrasts with observations made with GluRD, for which Ni^{2+} proved the most suitable cation (*11*). In our case, the improvement in purity appears to reflect a reduction of nonspecific binding of contaminants to the Zn^{2+} column. Although the binding of the hexahistidine tag was also weakened, consistent with peptide-binding experiments (*24*), the specificity of the interaction increased, permitting recovery of protein at much higher purity. Expression in High Five rather than Sf21 cells and harvest by continuous-flow centrifugation were important in minimizing protein aggregation, which had limited the usefulness of earlier glutamate receptor preparations from insect cells (*11*). Continuous-flow centrifugation is commonly used to harvest bacterial cells expressing recombinant proteins. However, our results suggest that it also may be an attractive alternative to batch centrifugation for pilot-scale expression of membrane proteins in the baculovirus system, where it has not yet found wide application.

GluRB yields a single peak in density-gradient centrifugation (Figure 3), confirming the uniformity of the oligomeric assembly. Although the peak is slightly broader than those of the standard proteins, this additional broadening may reflect heterogeneity in the TX-100 micelles, which typically range in size from 63 to 97 kDa (*25*). Assuming that one ~80 kDa micelle is bound per complex, the observed 495 kDa molecular mass of the complex corresponds well to that expected for a tetrameric molecule (4×104 kDa + 80 kDa = 496 kDa). In contrast, a pentameric glutamate receptor should have a molecular mass of at least 580 kDa (520 kDa protein + ≥60 kDa detergent). Hence we conclude that the recombinant GluRB most likely forms a tetramer.

This finding is consistent with a growing body of electrophysiological and biochemical evidence that supports a tetrameric assembly for GluR (*26*−*29*). Such an assembly would be expected on the basis of the homology of the GluR transmembrane domains to tetrameric potassium channels (*30*−*32*). Our measurement is, however, inconsistent with experiments that suggest a pentameric stoichiometry, particularly for *N*-methyl-D-aspartate-selective GluR (*33*−*35*).

Single-particle images of the GluRB homomers in negative stain suggest that the ion channel is an elongated structure with solvent-accessible internal features (Figure 4), some of which may correspond to ion-conducting pathways in the channel. The distribution of perspectives and observed anisotropy of the particle are reminiscent of the voltage-gated sodium channel (*36*). The dimensions of the particle are consistent with its molecular weight and could accommodate a tetrameric assembly of ~100 kDa protomers. The unequal particle dimensions are not consistent with a 4-fold symmetrical molecular assembly but would be consistent with internal 2-fold symmetry. To reconcile this observation with the presence of four subunits in the channel, one can speculate that the receptor may be assembled as a dimer of dimers, consistent with recent biochemical studies on the assembly of chimeric AMPA/kainate receptor subunits (*8*) and with the observation that the ligand-binding domain typically crystallizes in a dimeric form (*9*). The proposed 2-fold symmetry cannot be seen in the input projections (Figure 4C); however, symmetry can be masked by the orientations adopted by the particles on the film, as it was for most single-particle images of the 4-fold symmetric sodium channel (*36*). In our case, the putative internal symmetry axis may be preferentially oriented parallel to the plane of the carbon film and therefore inaccessible to direct visualization by electron microscopy.

A three-dimensional reconstruction of the molecular envelope of the GluRB homomer by angular reconstitution has been performed (data not shown). However, due to an unfavorable spatial distribution of perspectives and the lack of clear molecular symmetry that could be imposed during angular reconstitution, we cannot reliably interpret features beyond those that are visible in the input projections (Figure 4C). Nevertheless, good agreement between the model and the input projections confirms that the single GluRB channels were correctly preserved and imaged in negative stain and that the different class sums represent distinct perspectives of a single molecular structure. Thus, potential artifacts of the negative stain technique (e.g., partial staining and flattening; see ref *37*) appear to have been minimized. This being the case, other experimental approaches are available

to deal with limited perspectives. In the random conical tilt reconstruction technique, collection of pairs of electron micrographs of tilted and untilted particles provides a set of perspectives for each class of particles sufficient to determine independent 3D reconstructions for each class (*38*). Similar reconstructions can be merged, providing a relatively complete set of perspectives on the particle. Imaging particles in vitrified buffer or stain may yield additional, complementary perspectives and provide an independent check on the absence of staining artifacts in the reconstruction. Alternatively, if we can independently identify the molecular symmetry (e.g., from a random conical tilt reconstruction), then that symmetry can also be used to improve the reconstruction of untilted images by angular reconstitution.

We have purified functional, recombinant GluRB homomers that reveal a probable tetrameric stoichiometry and an elongated structure that would be consistent with a dimer-of-dimers assembly for these ion channels. The protein is well-suited to further biochemical and structural analysis. In particular, antibody labeling of known sequence epitopes should permit assignment of domains within an improved molecular envelope. Furthermore, the ability to express milligram quantities of high-quality material should support two-dimensional crystallization and functional reconstitution experiments designed to provide higher resolution structural and functional data, respectively.

ACKNOWLEDGMENT

We thank V. Bader and H. Clasen for skillful technical assistance, Drs. K. C. Holmes and R. R. Schröder (Department of Biophysics, MPI, Heidelberg) for making available the EM facilities, Dr. M. Schatz (Image Science Software GmbH, Berlin) for helpful discussions, and Dr. G. A. Scarborough (UNC, Chapel Hill) for helpful suggestions on the manuscript. We gratefully acknowledge the initial and continuing support of this project by Dr. B. Sakmann (Department of Cell Physiology, MPI, Heidelberg).

REFERENCES

1. Dingledine, R., Borges, K., Bowie, D., and Traynelis, S. F. (1999) *Pharm. Rev. 51*, 7−61.
2. Rose, C. R., and Konnerth, A. (2000) *Nature 405*, 413−415.
3. Hollmann, M., O'Shea-Greenfield, A., Rodgers, S. W., and Heinemann, S. (1989) *Nature 342*, 643−648.
4. Keinänen, K., Wisden, W., Sommer, B., Werner, P., Herb, A., Verdoorn, T. A., Sakmann, B., and Seeburg, P. H. (1990) *Science 249*, 556−560.
5. Boulter, J., Hollmann, M., Shea-Greenfield, O. A., Hartley, M., Deneris, E., Maron, C., and Heinemann, S. (1990) *Science 249*, 1033−1037.
6. Hollmann, M., Hartley, M., and Heinemann, S. (1991) *Science 252*, 851−853.
7. Osten, P., Khatri, L., Perez, J. L., Kohr, G., Giese, G., Daly, C., Schulz, T. W., Wensky, A., Lee, L. M., and Ziff, E. B. (2000) *Neuron 27*, 313−325.
8. Ayalon, G., and Stern-Bach, Y. (2001) *Neuron 13*, 103−113.
9. Armstrong, N. A., and Gouaux, E. (2000) *Neuron 28*, 165−181.
10. Keinänen, K., Kohr, G., Seeburg, P. H., Laukkanen, M. L., and Oker-Blom, C. (1994) *Bio/Technology 12*, 802−806.
11. Kuusinen, A., Arvola, M., Oker-Blom, C., and Keinänen, K. (1995) *Eur. J. Biochem. 233*, 720−726.
12. Hopp, T. P., Prickett, K. S., Price, V. L., Libby, R. T., March, C. J., Cerretti, D. P., Urdal, D. L., and Conlon, P. J. (1988) *Bio/Technology 6*, 1204.
13. Schiöth, H. B., Kuusinen, A., Muceniece, R., Szardenings, M., Keinänen, K., and Wikberg, J. E. (1996) *Biochem. Biophys. Res. Commun. 221*, 807−814.
14. Madden, D. R., Abele, R., Andersson, A., and Keinänen, K. (2000) *Eur. J. Biochem. 267*, 4281−4289.
15. Cheng, Y., and Prusoff, W. H. (1973) *Biochem. Pharmacol. 22*, 3099−3108.
16. Bradford, M. M. (1976) *Anal. Biochem. 72*, 248−254.
17. Schatz, M., Orlova, E. V., Dube, P., Jäger, J., and van Heel, M. (1995) *J. Struct. Biol. 114*, 28−40.
18. Serysheva, I. I., Orlova, E. V., Chiu, W., Sherman, M. B., Hamilton, S. L., and van Heel, M. (1995) *Nat. Struct. Biol. 2*, 18−24.
19. van Heel, M., Harauz, G., and Orlova, E. V. (1996) *J. Struct. Biol. 116*, 17−24.
20. Dube, P., Tavares, P., Lurz, R., and Van Heel, M. (1993) *EMBO J. 12*, 1303−1309.
21. Hollmann, M., and Heinemann, S. (1994) *Annu. Rev. Neurosci. 17*, 31−108.
22. Grisshammer, R., and Tate, C. G. (1995) *Q. Rev. Biophys. 28*, 315−422.
23. Abele, R., Lampinen, M., Keinänen, K., and Madden, D. R. (1998) *J. Biol. Chem. 273*, 25132−25138.
24. Yip, T. T., Nakagawa, Y., and Porath, J. (1989) *Anal. Biochem. 183*, 159−171.
25. Robson, R. J., and Dennis, E. A. (1977) *J. Phys. Chem. 81*, 1075−1078.
26. Laube, B., Kuhse, J., and Betz, H. (1998) *J. Neurosci. 18*, 2954−2961.
27. Mano, I., and Teichberg, V. I. (1998) *Neuroreport 9*, 327−331.
28. Rosenmund, C., Stern-Bach, Y., and Stevens, C. F. (1998) *Science 280*, 1596−1599.
29. Kuusinen, A., Abele, R., Madden, D. R., and Keinänen, K. (1999) *J. Biol. Chem. 274*, 28937−28943.
30. Chen, G.-Q., Cui, C., Mayer, M. L., and Gouaux, E. (1999) *Nature 402*, 817−821.
31. Wo, Z. G., and Oswald, R. E. (1995) *Trends Neurosci. 18*, 161−168.
32. Doyle, D. A., Cabral, J. M., Pfuetzner, R. A., Kuo, A., Gulbis, J. M., Cohen, S. L., Chait, B. T., and MacKinnon, R. (1998) *Science 280*, 69−77.
33. Ferrer-Montiel, A. V., and Montal, M. (1996) *Proc. Natl. Acad. Sci. U.S.A. 93*, 2741−2744.
34. Premkumar, L. S., and Auerbach, A. (1997) *J. Gen. Physiol. 110*, 485−502.
35. Hawkins, L. M., Chazot, P. L., and Stephenson, F. A. (1999) *J. Biol. Chem. 274*, 27211−27218.
36. Sato, C., Sato, M., Iwasaki, A., Doi, T., and Engel, A. (1998) *J. Struct. Biol. 121*, 314−325.
37. Cejka, Z., Kleinz, J., Santini, C., Hegerl, R., and Magaldi, A. G. (1992) *J. Struct. Biol. 109*, 52−60.
38. Radermacher, M. (1988) *J. Electron Micros. Technol. 9*, 359−394.

BI011143G